RESISTIVE HOSE INSTABILITY IN A DICHROMATIC ELECTRON BEAM

HAN S. UHM

NSWC MP 84–344

PLASMA PHYSICS PUBLICATION NO. 84-6

AUGUST 1984

NAVAL SURFACE WEAPONS CENTER

White Oak , Silver Spring, Maryland 20910

Accession Number: 5141

Publication Date: Aug 01, 1984

Title: Resistive Hose Instability In A Dichromatic Electron Beam

Personal Author: Uhm, H.

Corporate Author Or Publisher: Naval Surface Weapons Center, White oak Silver Spring, MD 20910
Report Number: NSWC MP 84-344 Report Number Assigned by Contract Monitor: STARL

Comments on Document: STARLAB RRI

Descriptors, Keywords: Hose Dichromatic Electron Beam Weapon Resistive Collision Plasma Channel Equilibrium Density Bennett Profile Pulse Growth Length Transport Distance Primary Secondary Energy Stability Property

Pages: 28

Cataloged Date: Jul 06, 1994

Document Type: HC

Log Number: SLL-85-U-310

Number of Copies In Library: 000001

Record ID: 28996

Source of Document: RRI

RESISTIVE HOSE INSTABILITY IN A DICHROMATIC ELECTRON BEAM

Han S. Uhm
Naval Surface Weapons Center
White Oak, Silver Spring, Maryland 20910

Stability properties of the resistive hose instability are investigated for a self-pinched dichromatic electron beam propagating through a collisional plasma channel. The equilibrium and stability analysis is carried out for the electron distribution function in which beam electrons have two energy components. The beam density is assumed to be a Bennett profile. A closed algebraic dispersion relation of the resistive hose instability is obtained for a dichromatic beam, by making use of the energy group model. Numerical investigation of the dispersion relation is carried out for a ultra-relativistic electron beam. Unstable growth of the resistive hose instability along the beam frame coordinate is calculated. For an appropriate choice of the physical parameters, it is shown that the growth rate of instability in a dichromatic beam can be one third of that in a monochromatic beam, thereby tremendously increasing the beam pulse length for a stable propagation.

I. INTRODUCTION

In recent years, there is a large and growing literature on the resistive hose instability[1-7] in an intense relativistic electron beam propagating through a collisional plasma channel. The resistive hose instability is a growing lateral distortion of a self-pinched electron beam, severely limiting the beam pulse length for a long range beam transport. Thus, we are often looking for appropriate physical parameters of the beam which may reduce the growth rate of instability, thereby enhancing the pulse length and propagation distance of the beam. In order to reduce the growth rate of instability, in this article we propose a new scheme which utilizes a dichromatic electron beam. The dichromatic electron beam consists of beam electrons with two energy components, so that the energy spectrum has double peaks. In this regard, this paper examines the resistive hose stability properties of a relativistic dichromatic electron beam.

A brief description of the equilibrium properties is presented in Sec. II for the equilibrim distribution function in which beam electrons have two energy components, the primary energy $\gamma_p mc^2$ and the secondary energy $\gamma_s mc^2$. Stability analysis of the resistive hose instability in a dichromatic electron beam is carried out in Sec. IV, assuming that the electron beam has a Bennett profile. Making use of the energy group model[6], the dispersion relation [Eq. (29)] of the resistive hose instability in a dichromatic beam is obtained. As a special case, numerical investigation of this dispersion relation is carried out for a ultra-relativistic electron beam with $\gamma_p > \gamma_s >> 1$. Unstable growth of the resistive hose instability along the beam frame coordinate $\zeta = ct - z$ is calculated, where ζ represents the axial coordinate

from the head of the beam to the tail. One of the most important features in the stability analysis is that the maximum growth rate of the resistive hose instability can be considerably reduced for a dichromatic beam. For an appropriate choice of the various physical parameters, it is shown that the growth rate of instability in a dichromatic beam is about one third of that in a monochromatic beam, thereby increasing the beam pulse length three times of its original value. We therefore conclude that the resistive hose perturbations in a dichromatic beam can be substantially suppressed.

II. EQUILIBRIUM DESCRIPTION

The equilibrium configuration consists of a relativistic electron beam propagating through a collisional plasma channel. The energy of the beam has two major components; the primary and secondary energies denoted by $\gamma_p mc^2$ and $\gamma_s mc^2$, respectively, where m is electron rest mass and c is the speed of light in vacuum. Cylindrical polar coordinates (r, θ, z) are introduced with the z-axis coinciding with the axis of symmetry, r is the radial distance from the z-axis and θ is the polar angle in a plane perpendicular to the z-axis. All beam equilibrium properties are assumed to be azimuthally symmetric ($\partial/\partial\theta = 0$) and independent of axial coordinate ($\partial/\partial z = 0$). In the present analysis, we investigate equilibrium and stability properties associated with the steady-state ($\partial/\partial t = 0$) beam distribution function,

$$f_b^0(H, P_\theta, P_z)$$

$$= \frac{n_p}{2\pi\gamma_p mT_p} \exp\left(-\frac{H - \gamma_p mc^2}{T_p}\right) \delta(P_z - \gamma_p m\beta_p c)$$

$$+ \frac{n_s}{2\pi\gamma_s mT_s} \exp\left(-\frac{H - \gamma_s mc^2}{T_s}\right) \delta(P_z - \gamma_s m\beta_s c), \qquad (1)$$

where n_p and n_s are the number densities of the primary and secondary energy components at r = 0, T_p and T_s are the corresponding temperatures, and $\beta_p c$ and $\beta_s c$ are the corresponding axial velocities of electrons with the primary and secondary energy components, respectively. In Eq. (1), the total energy

$$H = \gamma mc^2 = \left(m^2c^4 + c^2p^2\right)^{1/2}, \qquad (2)$$

the axial canonical momentum

$$P_z = p_z - (e/c)A_0(r), \tag{3}$$

and the canonical angular momentum $P_\theta = rp_\theta$ are the three single-particle constants of the motion, $p = (p_r, p_\theta, p_z)$ is the mechanical momentum, -e is the electron charge and $A_0(r)$ is the axial component of the equilibrium vector potential.

The equilibrium vector potential associated with the self-generated azimuthal magnetic field $B_\theta^0(r)$ is determined from Ampere's law

$$\frac{1}{r}\frac{d}{dr}\, r\, \frac{d}{dr} A_0(r) = -\frac{1}{r}\frac{d}{dr}\left[rB_\theta^0(r)\right] = \frac{4\pi e}{c}(1 - f)n_b^0(r)V_z^0(r) \tag{4}$$

where $n_b^0(r)$ is the equilibrium beam density profile, $V_z^0(r)$ is the equilibrium axial velocity and f is the fractional current neutralization assuming that the equilibrium plasma return current has the same radial profile as the beam current. It is assumed that the beam is completely space charge neutralized by the background plasma. In addition, we also assume that the motion of the beam electrons is paraxial, i.e., $p_\perp^2 = p_r^2 + p_\theta^2 << p_z^2$, which requires

$$\nu/\gamma_s << 1, \tag{5}$$

where ν is Budker's parameter defined by $\nu = N_b e^2/mc^2$ and N_b is the number of beam electrons per unit axial length.

Using the paraxial approximation, it follows that the combinations $H - \gamma_p mc^2$ and $H - \gamma_s mc^2$ can be approximated by

$$H - \gamma_p mc^2 = p_\perp^2/2\gamma_p m + e\beta_p A_0(r),$$

$$H - \gamma_s mc^2 = p_\perp^2/2\gamma_s m + e\beta_s A_0(r), \tag{6}$$

where $p_\perp^2 = p_r^2 + p_\theta^2$. Substituting Eq. (6) into Eq. (1) and carrying out the momentum integration give the beam density profile

$$n_b^0(r) = n_p \exp\left(-\frac{e\beta_p A_0}{T_p}\right) + n_s \exp\left(-\frac{e\beta_s A_0}{T_s}\right). \tag{7}$$

For simplification in the subsequent analysis, the beam temperature parameters T_p and T_s are restricted to

$$\beta_p T_s = \beta_s T_p, \tag{8}$$

thereby further simplifying Eq. (7) by

$$n_b^0(r) = (n_p + n_s) \exp(-e\beta_p A_0/T_p). \tag{9}$$

The condition in Eq. (8) can be easily satisfied for relativistic beams. Similarly, the axial component of the equilibrium beam current density profile is given by

$$J_b^0(r) = en_b^0(r)V_{bz}^0(r) = en_p\beta_p c(1 + \eta) \exp\left(-\frac{e\beta_p A_0}{T_p}\right), \tag{10}$$

where the density ratio η is defined by

$$\eta = n_s\beta_s/n_p\beta_p. \tag{11}$$

Combining Eqs. (4) and (10), we find that the axial component of the equilibrium vector potential $A_0(r)$ satisfies

$$\frac{1}{r}\frac{d}{dr}\, r\, \frac{d}{dr} A_0(r) = 4\pi e(1 - f)n_p\beta_p(1 + \eta)\, \exp(-\frac{e\beta_p A_0}{T_p}). \tag{12}$$

Therefore, once the vector potential $A_0(r)$ is determined from the nonlinear differential equation (12), the equilibrium self magnetic field $B_\theta^0(r) = -\partial A_0/\partial r$ can be calculated self-consistently from this vector potential and the beam current density profile $J_b^0(r)$ from Eq. (10). Defining the Bennett radius a of the dichromatic beam by

$$a^2 = \frac{2T_p}{\pi e^2 n_p(1 - f)\beta_p^2(1 + \eta)}, \tag{13}$$

it is straightforward to find that the solution of Eq. (12) is expressed as

$$A_0(r) = 2\,\frac{T_p}{e\beta_p}\, \ell n(1 + r^2/a^2), \tag{14}$$

which gives the beam current density profile

$$J_b^0(r) = \frac{en_p\beta_p c(1 + \eta)}{(1 + r^2/a^2)}. \tag{15}$$

From Eqs. (13) and (15), we note that increase of the number (η) of beam electrons with secondary energy component not only increases the total beam current density but also reduces beam radius considerably.

From Eq. (14), we obtain the equilibrium azimuthal field

$$B_\theta^0(r) = -2\pi e n_p (1 - f)\beta_p (1 + \eta) \frac{r}{1 + r^2/a^2}. \tag{16}$$

For convenience in the subsequent analysis, we define the betatron frequency $\omega_{\beta p}(r)$ of the primary energy beam electrons by

$$\omega_{\beta p}^2(r) = -\frac{e\beta_p B_\theta^0(r)}{\gamma_p m r} = \frac{\hat{\omega}_{\beta 0}^2}{1 + r^2/a^2}, \tag{17}$$

where the maximum betatron frequency-squared $\hat{\omega}_{\beta 0}^2$ is given by

$$\hat{\omega}_{\beta 0}^2 = 2\pi e^2 n_p \beta_p^2 (1 - f)(1 + \eta)/\gamma_p m. \tag{18}$$

Similarly, the betatron frequency $\omega_{\beta s}(r)$ of the secondary energy beam electrons is given by

$$\omega_{\beta s}^2(r) = \xi \frac{\hat{\omega}_{\beta 0}^2}{1 + r^2/a^2}, \tag{19}$$

where the mass ratio ξ is defined by

$$\xi = \gamma_p \beta_s / \gamma_s \beta_p. \tag{20}$$

It is obvious from Eqs. (17) - (20) that the betatron frequency of the primary energy electrons is much less than that of the secondary energy electrons for $\gamma_p >> \gamma_s$. Hugh difference between the betatron frequencies $\omega_{\beta p}(r)$ and $\omega_{\beta s}(r)$ provides a strong stabilizing influence on the resistive hose instability as will be seen in the next section.

III. HOSE STABILITY ANALYSIS

In this section, we derive the dispersion relation of the resistive hose instability in a dichromatic beam by making use of the energy group model.[6] Adopting a normal mode approach, all perturbed quantities are assumed to vary with θ, z and t according to

$$\psi(\underset{\sim}{x},t) = \hat{\psi}(r)\exp\{i(\theta + kz - \omega t)\},$$

where k is the axial wavenumber and ω is the frequency. It is further assumed that the perturbed beam space charge field is completely neutralized by the plasma, i.e., $4\pi\sigma(r) >> \omega$, where $\sigma(r)$ is the scalor conductivity of the plasma. We also consider long wavelength and low frequency perturbations satisfying $|ka| << 1$ and $|\omega a| << c$, where a is the Bennett radius of the beam defined in Eq. (13)., Thus, the transverse electric components of the perturbed field, B_z, E_r and E_θ, can be neglected, and the perturbation can be represented in terms of the axial component of the perturbed vector potential $\hat{A}(r)$. After some algebraic manipulation, Ampere's law for $\hat{A}(r)$ is expressed as

$$\frac{d}{dr}\frac{1}{r}\frac{d}{dr}[r\hat{A}(r)] + \frac{4\pi i\omega\sigma(r)}{c^2}\hat{A}(r) = -\frac{4\pi}{c}\hat{J}_b(r), \qquad (21)$$

where $\hat{J}_b(r)$ is the perturbed axial beam current density.

It is worthwhile to identify portions of the equilibrium beam current density in Eq. (15), i.e.,

$$J_b^0(r) = J_p^0(r) + J_s^0(r), \tag{22}$$

which originates from the primary (J_p^0) and secondary (J_s^0) energy electrons. Substituting Eq. (11) into Eq. (15), we recognize

$$J_p^0(r) = \frac{en_p\beta_p c}{\left(1 + r^2/a^2\right)^2},$$

$$J_s^0(r) = \frac{en_s\beta_s c}{\left(1 + r^2/a^2\right)^2}. \tag{23}$$

According to the energy group model[6], the perturbed axial current density $J_b^0(r)$ is expressed as

$$\hat{J}_b(r) = -\frac{e\beta_p}{\gamma_p m}\frac{\hat{A}(r)/r}{\Omega_p^2 - \omega_{\beta p}^2(r)}\frac{d}{dr}J_p^0(r)$$

$$-\frac{e\beta_s}{\gamma_s m}\frac{\hat{A}(r)/r}{\Omega_s^2 - \omega_{\beta s}^2(r)}\frac{d}{dr}J_s^0(r), \tag{24}$$

where the Doppler-shifted eigenfrequency Ω_p and Ω_s of the primary and secondary energy electrons are defined by

$$\Omega_p = \omega - k\beta_p c, \qquad \Omega_s = \omega - k\beta_s c. \tag{25}$$

Consistent with the energy group model, the eigenfunction is approximated by

$$\hat{A}(r) = \int_0^\infty dRR\left[\frac{d}{dR}J_b^0(R)\right]\delta A(r;R), \tag{26}$$

where the component eigenfunction is given by

$$\delta A(r;R) = \begin{cases} r/R, & 0 \leq r \leq R, \\ R/r, & r > R. \end{cases}$$

Without loss of the generality, the component eigenfunction is normalized to unity at $r = R$. After a straightforward manipulation of Eq. (26), we obtain

$$\hat{A}(r) = \alpha \frac{r}{1 + r^2/a^2}, \tag{27}$$

where use has been made of Eq. (15) and α is an arbitrary constant. The plasma conductivity profile is assumed to be the Bennett profile

$$\sigma(r) = \frac{\hat{\sigma}}{(1 + r^2/a^2)^2}, \tag{28}$$

which is a reasonable assumption, since the plasma channel is created by the ionization of air molecules by the beam electrons and this ionization profile may be the same as the beam density profile.

We briefly summarize derivation of the dispersion relation of the resistive hose instability in a dichromatic beam. We substitute Eqs. (24) and (28) into the eigenvalue equation (21), and then multiply Eq. (21) by $r\hat{A}(r)$ [in Eq. (27)] and integrate over r from $r = 0$ to $r = \infty$. After a tedious algebraic calculation, it can be shown that the desired dispersion relation is expressed as

$$i\omega\tau_d = -\frac{f}{1-f} + \frac{6}{(1-f)(1+n)}\{y_s n[y_s - \frac{1}{2} + y_s(1-y_s)\,\ell n\,(\frac{y_s}{y_s-1}) + y_p\,[y_p - \frac{1}{2} + y_p(1-y_p)\ell n(\frac{y_p}{y_p-1})]\}, \tag{29}$$

where the parameter y_s and y_p are determined by

$$y_s = \xi\Omega_s^2/\hat{\omega}_{\beta 0}^2,\ y_p = \Omega_p^2/\hat{\omega}_{\beta 0}^2, \tag{30}$$

and the dipole magnetic decay time τ_d is defined by

$$\tau_d = \pi a^2\hat{\sigma}/2c^2. \tag{31}$$

Equation (29) is one of the main results of this paper and can be used to investigate the resistive hose stability properties of a dichromatic beam for a broad range of the physical parameters.

As a special case, subsequent analysis of the dispersion relation in Eq. (29) is restricted to a ultra-relativistic electron beam characterized by

$$\gamma_s >> 1. \tag{32}$$

Within the context of Eq. (32), the Doppler-shifted eigenfrequencies Ω_s and Ω_p are approximated by

$$\Omega = \omega - kc \approx \Omega_s \approx \Omega_p, \tag{33}$$

and the dispersion relation in Eq. (29) is simplified to

$$i\omega\tau_d = -\frac{f}{1-f} + \frac{6x}{(1-f)(1+\eta)}\{\eta\xi[\xi x - \frac{1}{2} + \xi x(1-\xi x)\ell n(\frac{\xi x}{\xi x - 1})] + x - \frac{1}{2} + x(1-x)\ell n(\frac{x}{x-1})\}, \tag{34}$$

where the parameter x is defined by

$$x = \Omega^2/\hat{\omega}_{\beta 0}^2. \tag{35}$$

The resistive hose stability properties of a dichromatic beam can be numerically investigated from Eq. (34), assuming either one of the frequencies ω and Ω as a explicitly given real value.

It is instructive to examine the present results in the three limiting cases. The dispersion relation in Eq. (34) is further simplified to

$$i\omega\tau_d = -\frac{f}{1-f} + \frac{6x}{1-f}[x - \frac{1}{2} + x(1-x)\ell n(\frac{x}{x-1})], \tag{36}$$

for $\eta = 0$ corresponding to the case of no secondary energy electrons or for $\xi = 1$ corresponding to the case when the primary and secondary energies are the same. For the case when there are no primary energy electrons, Eq. (34) can also be simplified to

$$i\omega\tau_d = -\frac{f}{1-f} + \frac{6\xi x}{1-f}[\xi x - \frac{1}{2} + \xi x(1-\xi x)\ell n(\frac{\xi x}{\xi x - 1})]. \tag{37}$$

Equations (36) and (37) are identical in forms to the result obtained by Lee[4].

III.A. Instability along the Beam Frame Coordinate

In this subsection, we investigate unstable growth of the resistive hose instability along the beam frame coordinate ζ defined by

$$\zeta = ct - z, \tag{38}$$

which represents the axial coordinate from the head of the beam to tail. The corresponding eigenfrequency to this coordinate is identified by ω. Therefore, the growth rate ω_i and real oscillation frequency ω_r are determined from the dispersion relation by numerically solving Eq. (34) for $\omega = \omega_r + i\omega_i$. Shown in Fig. 1 is plots of (a) the normalized growth rate $\omega_i \tau_d$ and (b) real oscillation frequency $\omega_r \tau_d$ versus $\Omega/\hat{\omega}_{\beta 0}$ obtained from Eq. (34) for $f = 0$, $\xi = 0.1$ and $\eta = 3$. The presentation in Fig. 1 is one of the typical plots of the growth rate and real frequency of the resistive hose instability in a dichromatic beam. Several points are noteworthy from Fig. 1. First, the growth rate of instability has two local maximum values. These local maximum growth rates occur at $\Omega/\hat{\omega}_{\beta 0} \approx 0.525$ corresponding to the maximum resonance value $x = 0.276$ for primary energy electrons and at $\Omega/\hat{\omega}_{\beta 0} \approx 1.66$ corresponding to the maximum resonance value $x = 0.276/\xi$ for secondary energy electrons. Second, the maximum growth rate of instability reduces considerably with dichromatic energies. Stabilizing influence of dichromatic energies is very obvious in the following physical consideration. Without secondary energy electrons, the maximum growth rate $\omega_i \tau_d = 0.69$ occurs at the resonance frequency corresponding to $x = 0.276$. Presence of the secondary energy electrons increases the betatron frequency-squared $\hat{\omega}^2_{\beta 0}$ of the primary energy electrons [Eq. (18)], thereby also enhancing the beam rigidity and eventually

reducing the growth rate of instability. On the other hand, the perturbations with the resonance frequency corresponding to $x = 0.276/\xi$ have maximum unstable interactions with the secondary energy electrons. However, the presence of the primary energy electrons with very low betatron frequency provides a strong damping mechanism for high resonance frequency. Third, the real oscillation frequency also has very different profile in comparison with that of the resistive hose instability in a monochromatic beam. The presentation in Fig. 1 clearly indicates that the instability nature is a mixture of the resistive hose instability of two monochromatic beams with different energies.

In order to illustrate the importance of the secondary energy electrons, Fig. 2 shows plots of the normalized growth rate $\omega_i \tau_d$ versus $\Omega/\hat{\omega}_{\beta 0}$ obtained from Eq. (34) for $f = 0$, $\xi = 0.1$ and several different values of η. The local maximum growth rate of instability associated with the resonance frequency of the primary energy electrons decreases from $\omega_i \tau_d = 0.69$ to zero with increasing value of η. On the other hand, the local maximum growth rate of instability associated with the resonance frequency of the secondary energy electrons increases from $\omega_i \tau_d = 0$ to $\omega_i \tau_d = 0.69$ when η increases from zero to infinity. Therefore for specified value of ξ, there is one optimum value of η for stability. Figure 3 presents plots of the normalized maximum growth rate $\omega_i \tau_d$ versus η obtained from Eq. (34) for $f = 0$, and several different values of ξ. For the case when the primary and secondary energies are the same $(\xi = 1)$, the normalized maximum growth rate is $\omega_i \tau_d = 0.69$ for an arbitrary value of η[Eq. (36)]. On the other hand for $\xi \neq 1$, the stability properties are very dependent of η. For example, for $\xi = 0.1$, the lowest maximum growth rate $\omega_i \tau_d = 0.235$ of instability occurs at $\eta = 3.2$. The growth

rate $\omega_i \tau_d = 0.235$ is approximately one third of the maximum growth rate of instability in a monochromatic beam. Finally, in Fig. 4, we also present plots of the normalized growth rate versus $\Omega/\hat{\omega}_{\beta 0}$ for f = 0.2 and parameters otherwise identical to Fig. 2. The stability behavior for a non-zero fractional current neutralization is similar to that for the f = 0 case, although the overall growth rate of instability for $f \neq 0$ is larger than that for f = 0 as expected.

III.B. Instability along the Laboratory Frame Coordinate z

For completeness of the stability analysis, in this section we briefly investigate unstable growth of the resistive hose instbility along the laboratory frame coordinate z (propagation range), i.e., we regard ω in Eq. (34) as a fixed real quantity and solve the dispersion relation for $\Omega = \Omega_r + i\Omega_i$ where Ω_r and Ω_i are the real frequency and growth rate, respectively, of instability. It is worthwhile to note that the dispersion relation in Eq. (34) is an even function of Ω. Therefore, if $\Omega = \Omega_r + i\Omega_i$ is a solution to Eq. (34), then $\Omega = -\Omega_r - i\Omega_i$ is also one of the solutions to Eq. (34) for a specified value of $\omega\tau_d$. Figure 5 presents plots of (a) the normalized growth rate $\Omega_i/\hat{\omega}_{\beta 0}$ and (b) real oscillation frequency $\Omega_r/\hat{\omega}_{\beta 0}$ versus $\omega\tau_d$ obtained from Eq. (34) for f = 0, $\eta = 3$, and $\xi = 0.1$ and $\xi = 1$. We remind the reader that the case of $\xi = 1$ corresponds to the resistive hose instability in a monochromatic beam [Eq. (36)]. In the laboratory frame, stability properties of the resistive hose instability in a dichromatic beam are similar to those in a monochromatic beam. However, the maximum growth rate of instability occurs at small value of $\omega\tau_d$ for a dichromatic beam.

IV. CONCLUSIONS

This paper has examined stability properties of the resistive hose instbility in a relativistic dichromatic electron beam propagating through a collision-dominated plasma channel. A brief description of the equilibrium properties has been presented in Sec. II for the equilibrium distribution function in which beam electrons have two energy components. Stability analysis of the resistive hose instability in a dichromatic electron beam was carried out in Sec. III, assuming that the electron beam has a Bennett density profile. The dispersion relation of the resistive hose instability in a dichromatic beam was obtained by making use of the energy group model. Numerical investigation of this dispersion relation was carried out for a ultra-relativistic electron beam. Unstable growth of the resistive hose instability along the beam frame coordinate ζ has been calculated. One of the most important features in this analysis is that the maximum growth rate of instability can be considerably reduced for a dichromatic beam. For an appropriate choice of the physical parameters, it has been shown that the growth rate of instability in a dichromatic beam can be one third of that in a monochromatic beam, thereby tremendously increasing the beam pulse length for a stable long range propagation.

ACKNOWLEDGEMENTS

This research was supported in part by the Independent Research Fund at the Naval Surface Weapons Center and in part by Naval Sea Systems Command.

We are grateful to Dr. C. M. Huddleston for his sustained interest in this work and for his suggestion of the title of this article.

REFERENCES

1. M. N. Rosenbluth, Phys. Fluids 3, 932 (1960).

2. E. P. Lee and L. D. Pearlstein, Phys. Fluids 16, 904 (1973).

3. S. Weinberg, J. Math. Phys. 5, 1371 (1964); J. Math. Phys. 8, 614 (1967).

4. E. P. Lee, Phys. Fluids 21, 1327 (1978).

5. E. J. Lauer, R. J. Briggs, T. J. Fessendon, R. E. Hester and E. P. Lee, Phys. Fluids 21, 1344 (1978).

6. H. S. Uhm and M. Lampe, Phys. Fluids 23, 1574 (1980).

7. W. M. Sharp, M. Lampe and H. S. Uhm, Phys. Fluids 25, 1456 (1982).

FIGURE CAPTIONS

Figure 1 — Plots of (a) normalized growth rate $\omega_i \tau_d$ and (b) real frequency $\omega_r \tau_d$ versus $\Omega/\hat{\omega}_{\beta 0}$ obtained from Eq. (34) for $f = 0$, $\xi = 0.1$ and $\eta = 3$.

Figure 2 — Plots of normalized growth rate $\omega_i \tau_d$ versus $\Omega/\hat{\omega}_{\beta 0}$ obtained from Eq. (34) for $f = 0$, $\xi = 0.1$ and several different values of η.

Figure 3 — Plots of normalized maximum growth rate $\omega_i \tau_d$ versus η obtained from Eq. (34) for $f = 0$, and several different values of ξ.

Figure 4 — Plots of normalized growth rate $\omega_i \tau_d$ versus $\Omega/\hat{\omega}_{\beta 0}$ obtained from Eq. (34) for $f = 0.2$ and parameters otherwise identical to Fig. 2.

Figure 5 — Plots of (a) normalized growth rate $\Omega_i/\hat{\omega}_{\beta 0}$ and (b) real oscillation frequency $\Omega_r/\hat{\omega}_{\beta 0}$ versus $\omega\tau_d$ obtained from Eq. (34) for $f = 0$, $\eta = 3$, and $\xi = 0.1$ and $\xi = 1$.

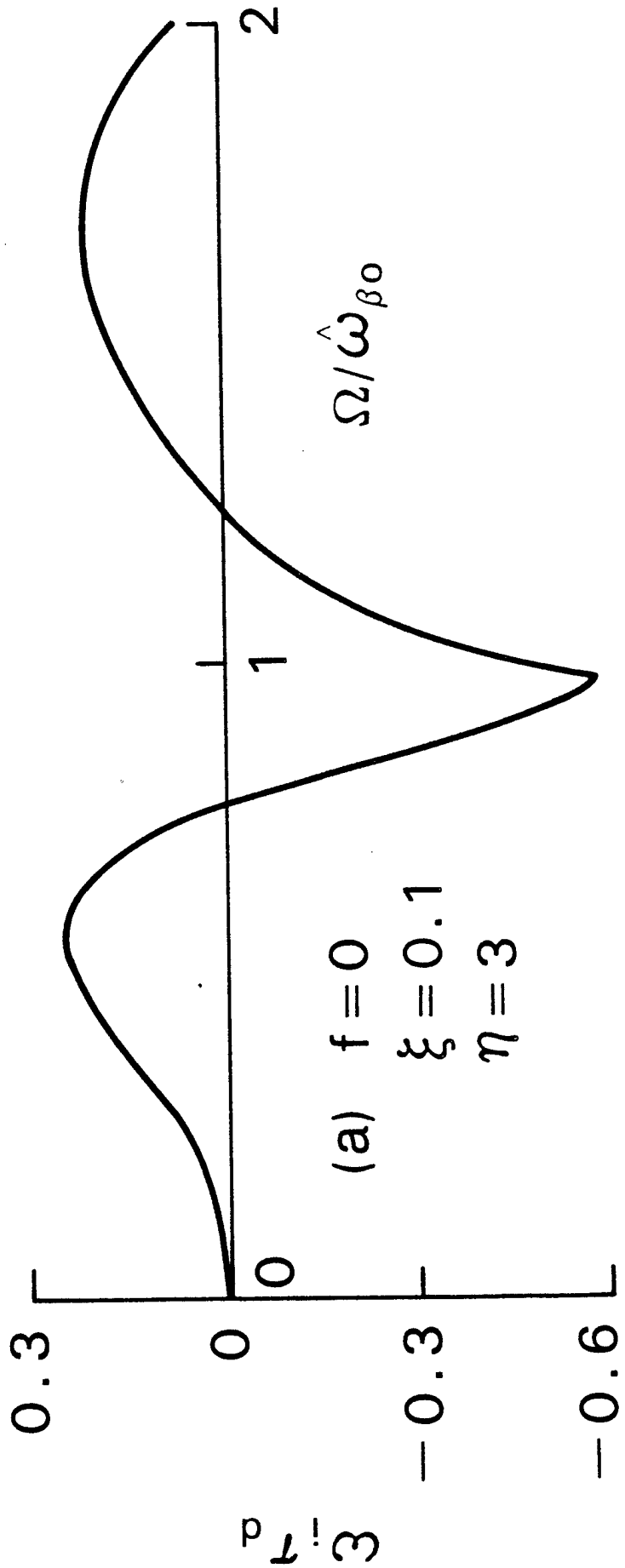

Figure 1a

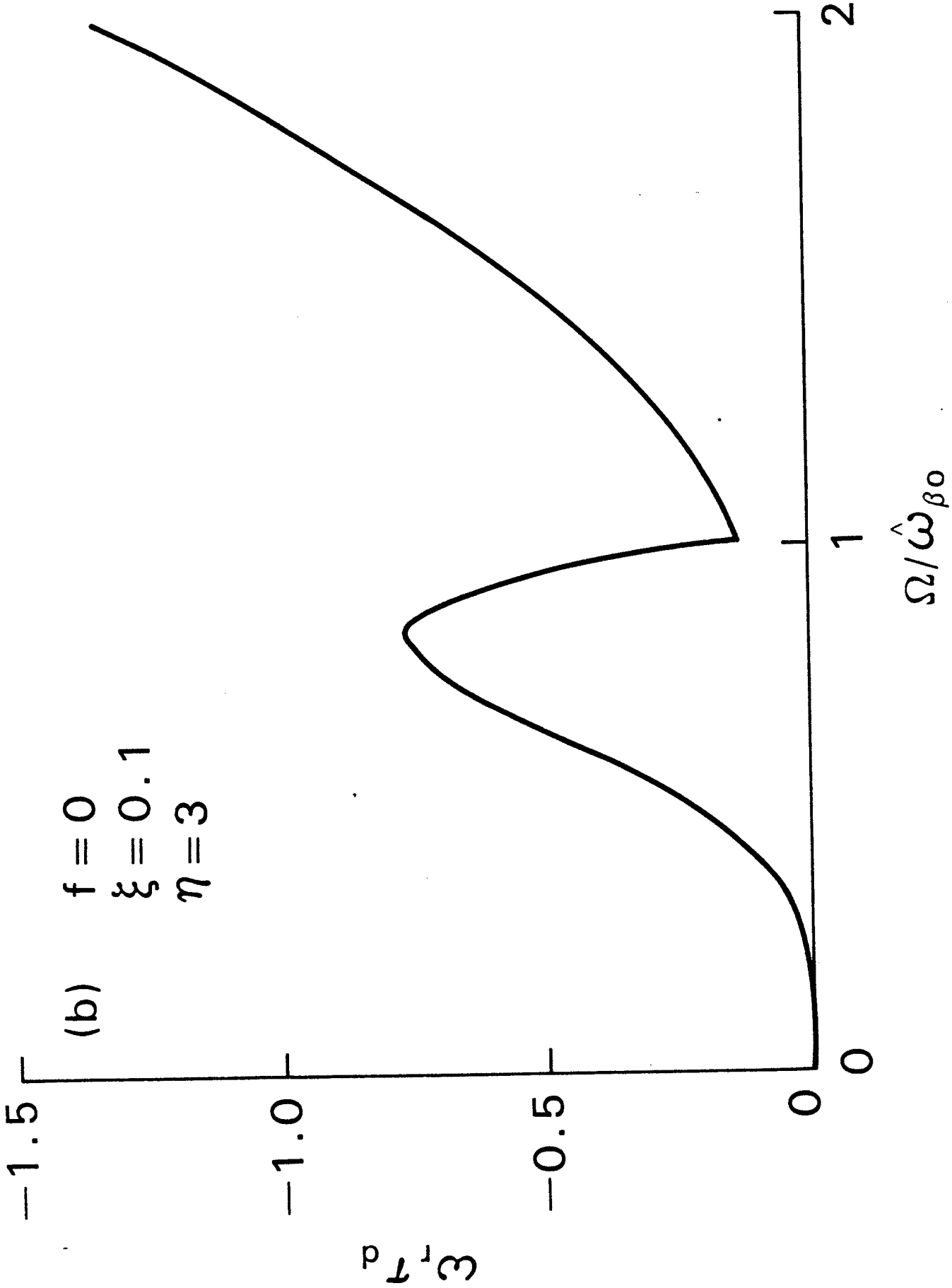
(b)
f = 0
ξ = 0.1
η = 3
$\varepsilon_r \tau_d$
−1.5
−1.0
−0.5
0
0
1
2
$\Omega/\hat{\omega}_{\beta o}$

Figure 1b

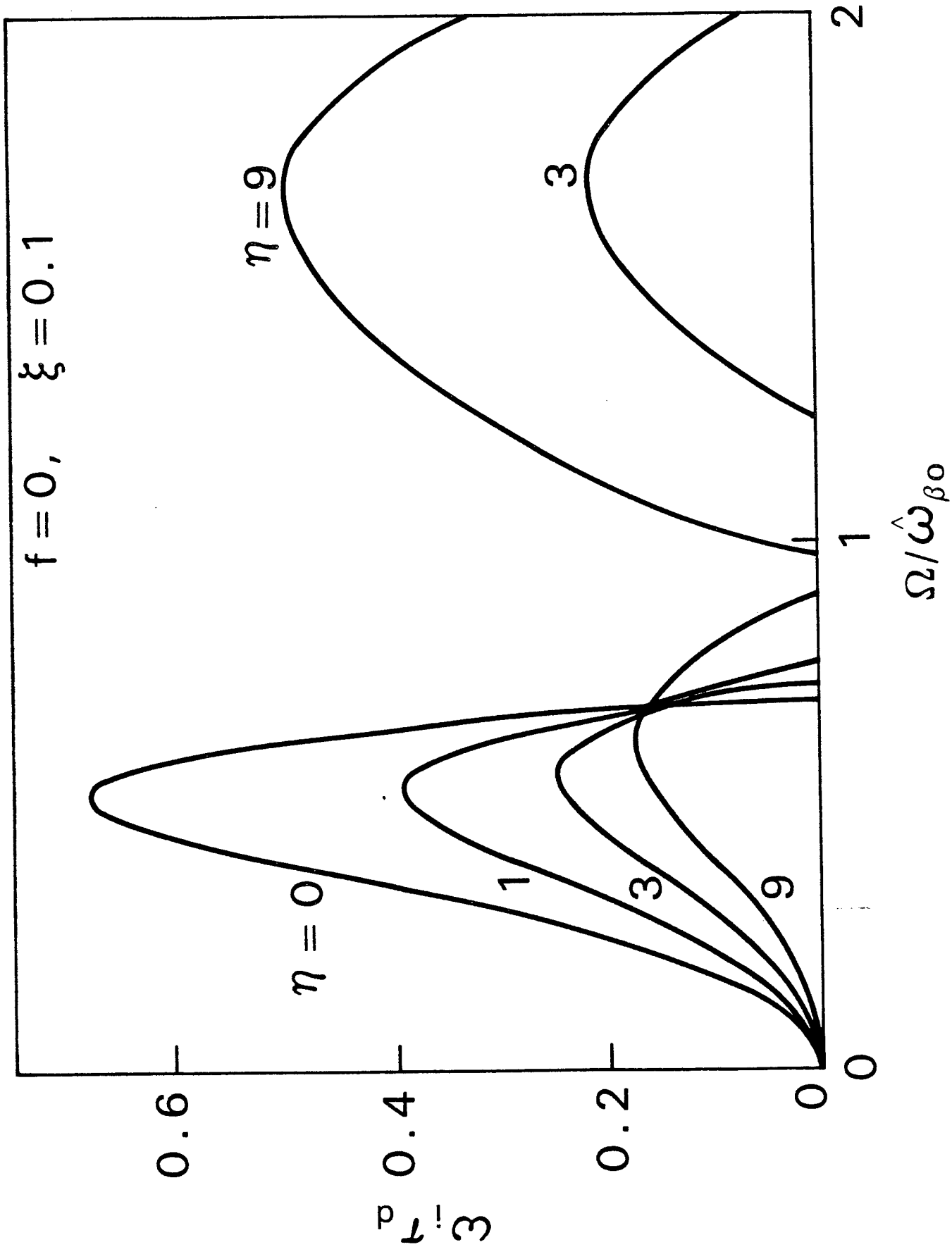

Figure 2

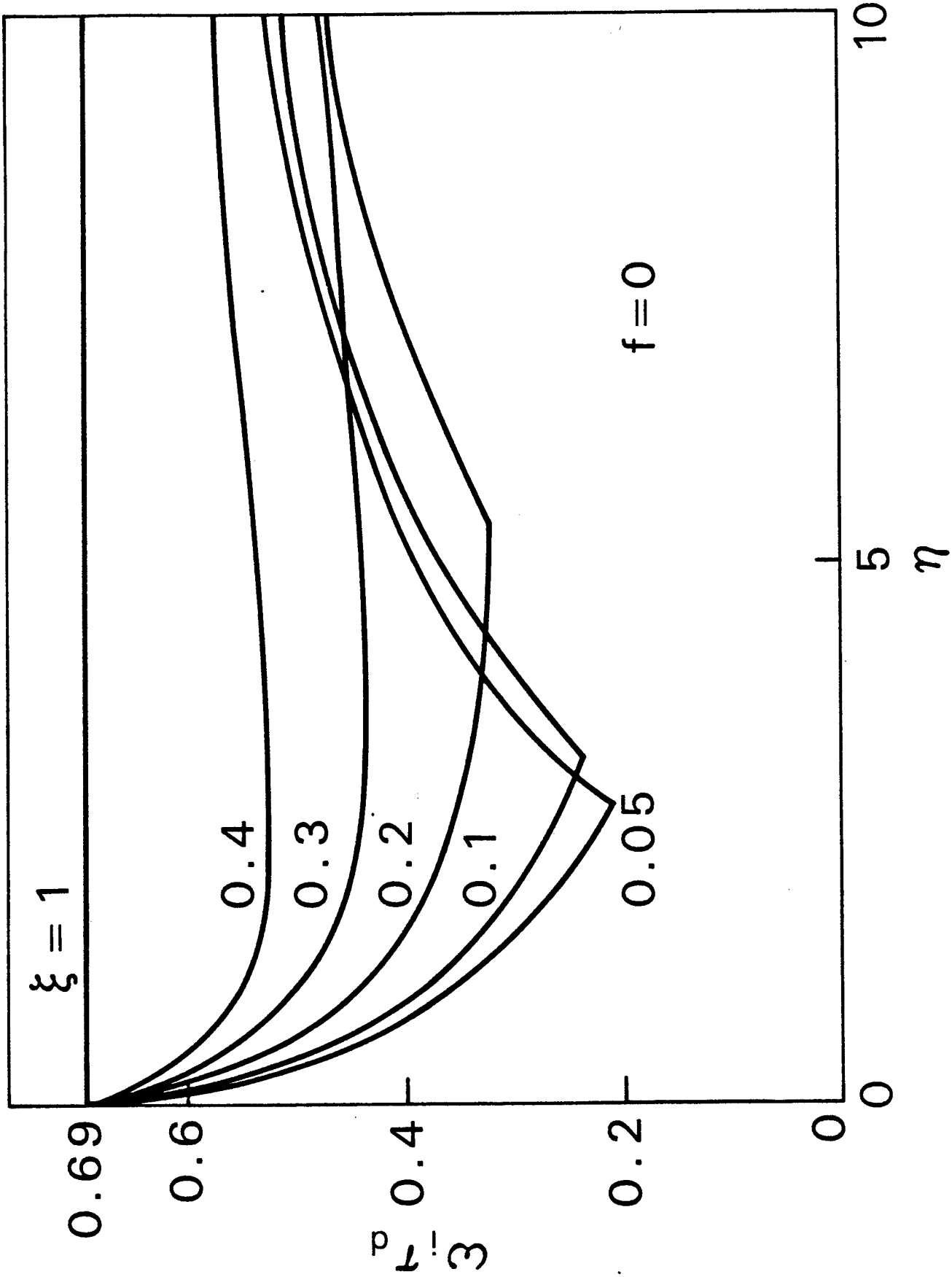

Figure 3

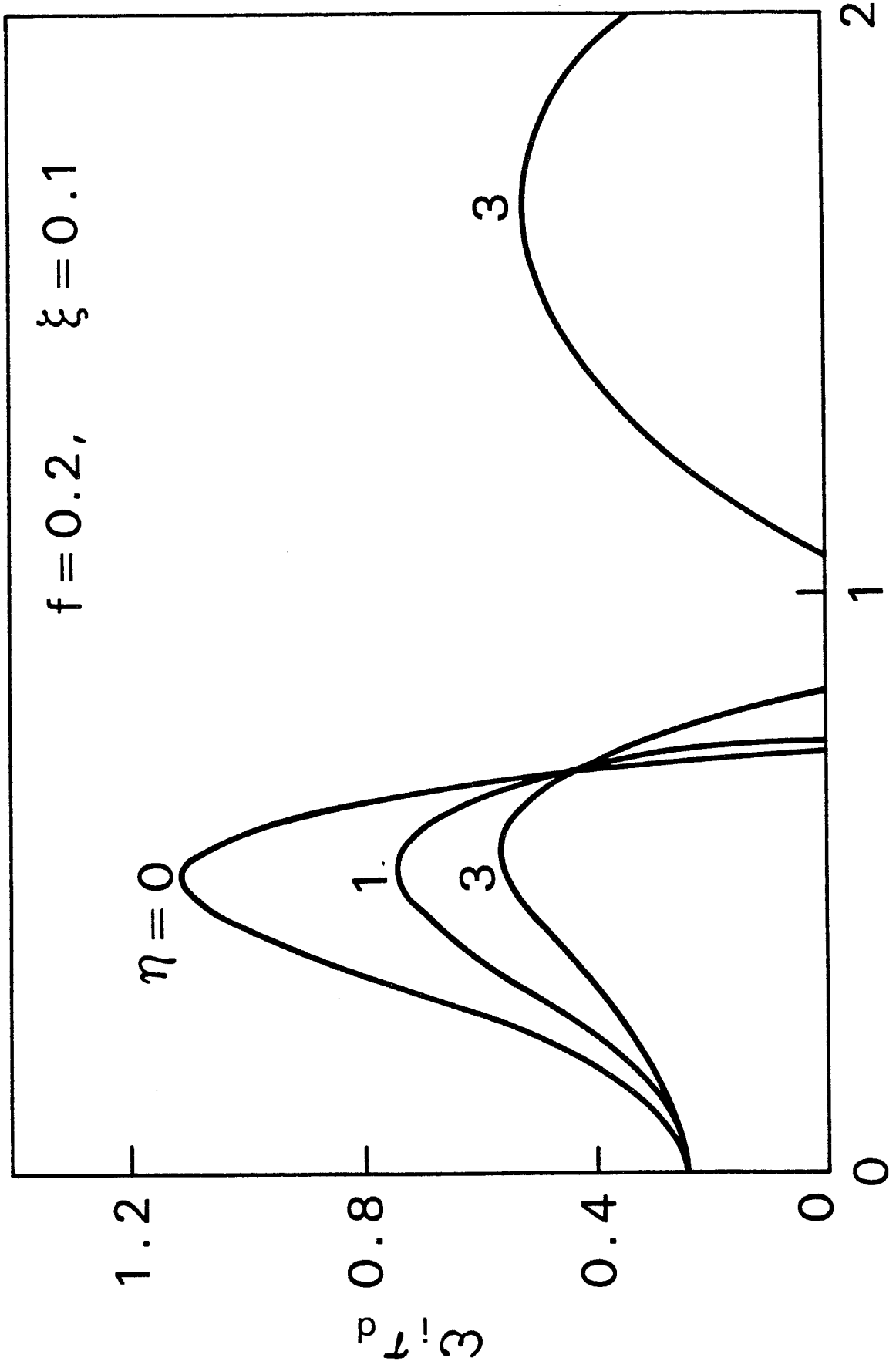

Figure 4

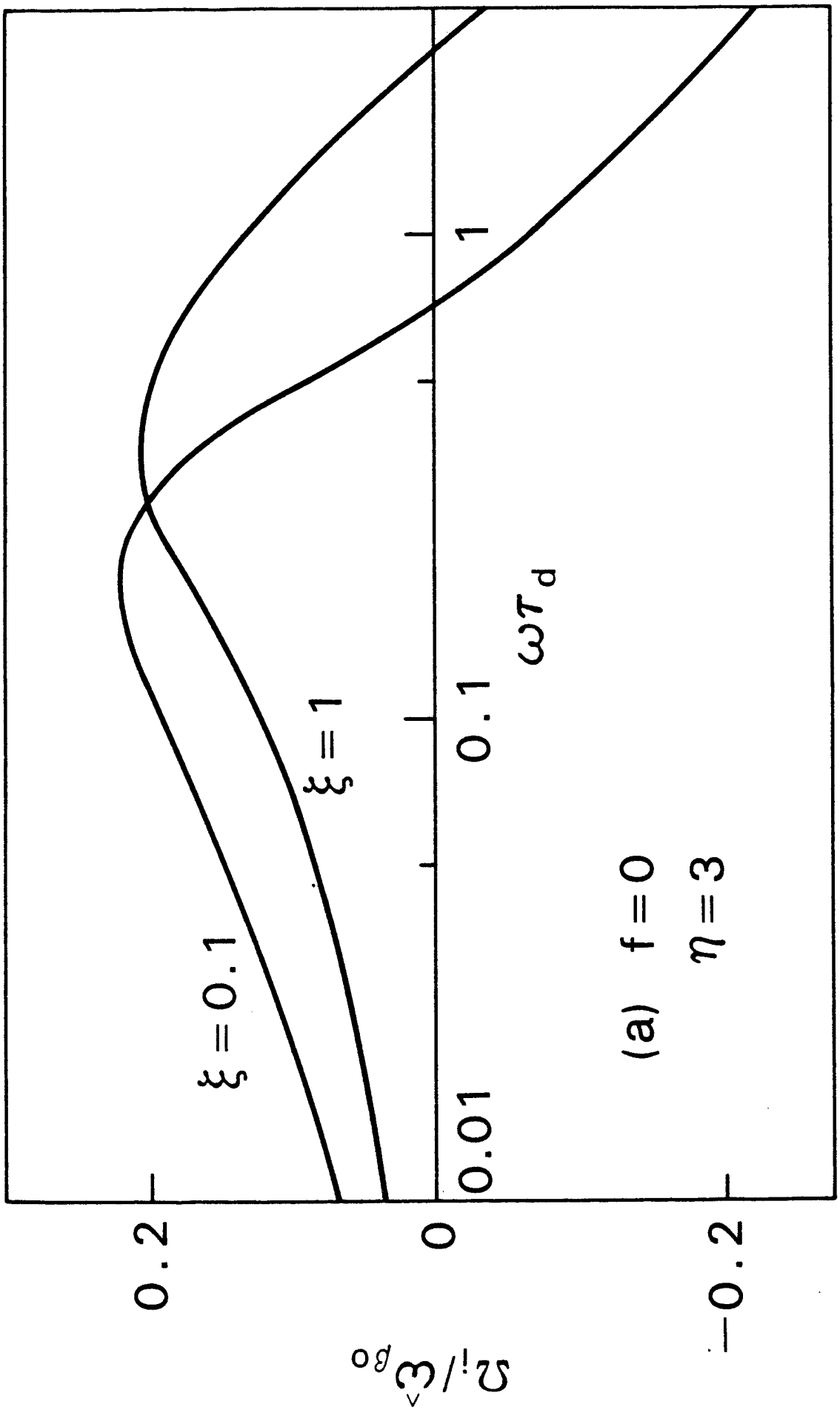

Figure 5a

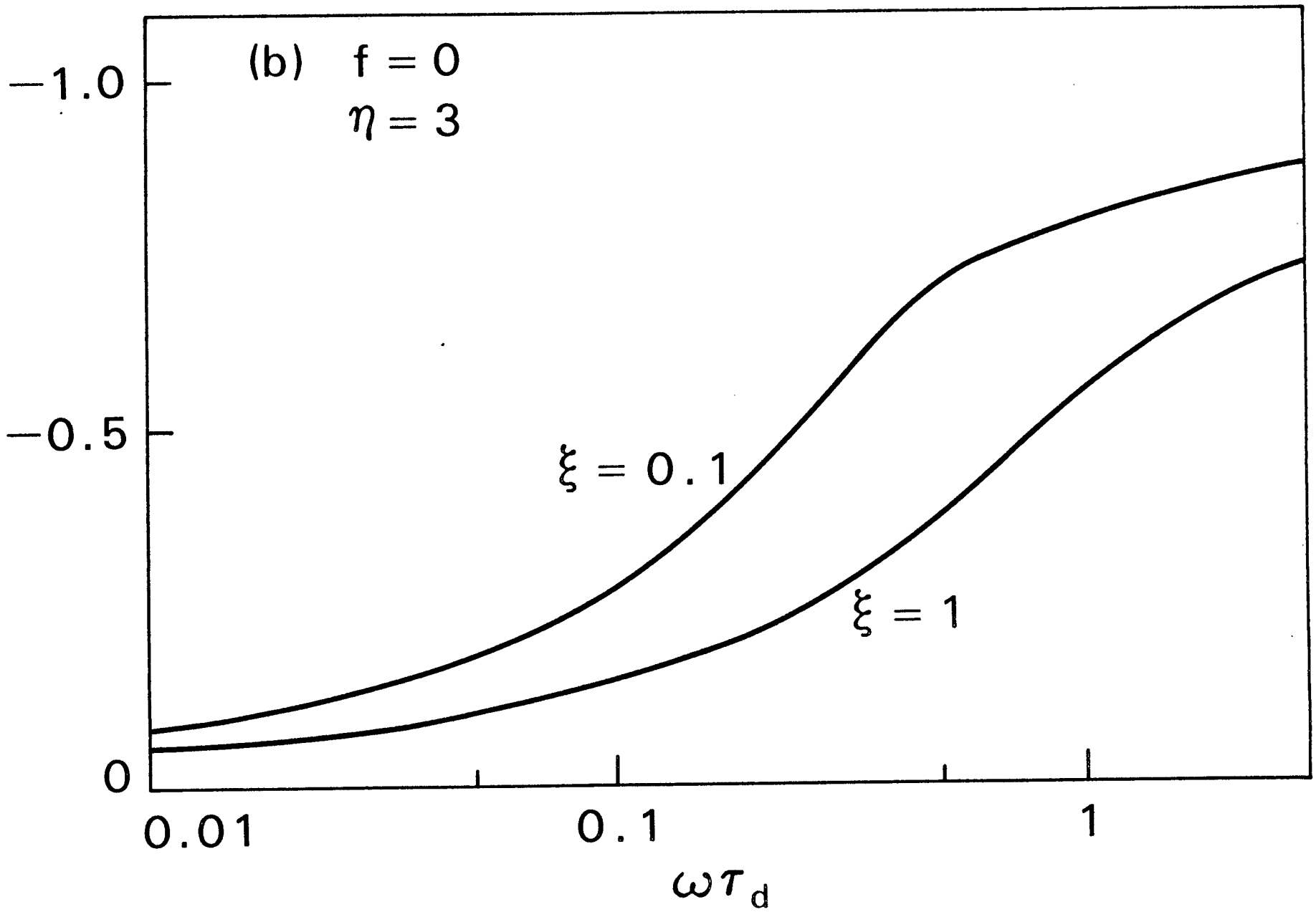

Figure 5b